PSFC/JA-00-37

Cross-Field Transport in the SOL: Its Relationship to Main Chamber and Divertor Neutral Control in Alcator C-Mod

B. LaBombard, B. Lipschultz, J.A. Goetz, C.S. Pitcher,
N. Asakura[1], R.L. Boivin, J.W. Hughes, A. Kallenbach[2],
G.M. McCracken[3], G.F. Matthews[3], D. Mossessian,
J.E. Rice, J.L. Terry, M.V. Umansky[4], and the Alcator Group

November 2000

Plasma Science and Fusion Center
Massachusetts Institute of Technology
Cambridge, MA 02139 USA

[1]Japan Atomic Energy Research Institute, Naka-Machi, Naka-gun, Ibareki-ken, Japan.
[2]MPI fur Plasmaphysik, EURATOM Association, D-85748 Garching, Germany.
[3]UKAEA Fusion, Culham Science Centre, Abingdon, Oxon, OX14 3EA.
[4]Laboratory for Laser Energetics, 250 East River Rd., Rochester, NY 14623 USA.

This work was supported by the U.S. Department of Energy, Cooperative Grant No. DE-FC02-99ER54512. Reproduction, translation, publication, use and disposal, in whole or in part, by or for the United States government is permitted.

Submitted to IAEA for publication of *18th IAEA Fusion Energy Conference Proceedings.* To be published on CD-ROM.

Cross-Field Transport in the SOL: Its Relationship to Main Chamber and Divertor Neutral Control in Alcator C-Mod

B. LaBombard, B. Lipschultz, J.A. Goetz, C.S. Pitcher, N. Asakura 1), R.L. Boivin, J.W. Hughes, A. Kallenbach 2), G.M. McCracken 3), G.F. Matthews 3), D. Mossessian, J.E. Rice, J.L. Terry, M.V. Umansky 4), Alcator group

M.I.T. Plasma Science and Fusion Center, 175 Albany St., Cambridge, MA 02139 USA.
1) Japan Atomic Energy Research Institute, Naka-Machi, Naka-gun, Ibareki-ken, Japan
2) MPI fur Plasmaphysik, EURATOM Association, D-85748 Garching, Germany
3) UKAEA Fusion, Culham Science Centre, Abingdon, Oxon., OX14 3EA
4) Laboratory for Laser Energetics, 250 East River Rd., Rochester, NY 14623 USA

e-mail: Labombard@psfc.mit.edu

Abstract: The sources of neutrals at the outer midplane of the plasma are discussed. We find that both the flux of neutrals escaping the divertor through leaks and ion recycling at main chamber surfaces appear to contribute. The ion flux to the walls is larger than the flux entering the divertor and comparable to recycling at the divertor plate. The cause of these high wall ion fluxes is an enhancement of cross-field particle transport which gives rise to substantial convective heat transport at higher densities. We have further explored main chamber recycling and impurity transport utilizing a novel divertor 'bypass', which connects the outer divertor plenum to the main chamber. We find that leakage of neutrals (fuel and recycling impurities) from the divertor appears to be determined primarily by the conductance through the divertor structure, thus indicating that tight baffling would be desirable in a reactor for fuel and helium ash compression.

1. Introduction

Magnetic divertors were originally conceived as a means for minimizing plasma-wall contact in the main chamber by redirecting the wall interaction to a chamber that is remote from the core plasma. In this ideal picture, all particle and heat fluxes which cross the magnetic separatrix result in flows along open field lines into the divertor chamber.

Experiments in Alcator C-Mod clearly demonstrate that this ideal description does not universally apply. Although the C-Mod divertor usually receives most of the conducted and convected energy fluxes from the Scrape-Off Layer (SOL) and does entrain/compress recycling impurity and fuel gases, a large fraction of ions in the SOL flow to the walls rather than *flow into* the divertor. The flux of ions that reach the divertor plates is much higher than the flux of ions entering the divertor (~x5) owing to the strong recycling *in* the divertor.

The reason for such high ion fluxes to the vessel walls rather than into the divertor appears to be primarily caused by the existence of strong cross-field particle transport in the main-chamber SOL. Cross-field particle transport in the SOL increases with distance from the separatrix, carrying particles to main-chamber wall surfaces rather than into the divertor volume [1]. ASDEX Upgrade also reports that main-chamber recycling, rather than divertor geometry, sets the midplane neutral pressure [2]. A further consequence of this phenomenon can be rapid cross-field heat convection in the SOL. Fusion reactors will likely operate similarly to Alcator C-Mod, with a baffled divertor geometry and fully saturated walls. Thus, the effects of enhanced cross-field transport and 'main-chamber recycling' on tokamak divertor operation need to be understood.

2. Experimental Arrangement

All results reported in this paper were obtained in deuterium discharges with a diverted, lower single-null magnetic equilibrium, and $B \times \nabla B$ ion drift directed towards the lower X-point. Detailed information on Alcator C-Mod's design, diagnostics, and operational characteristics can be found elsewhere [3].

The plasma-facing surfaces in Alcator C-Mod consist principally of molybdenum tiles. Boronization of internal surfaces is performed at regular intervals. For almost all discharges, the first-wall in Alcator C-Mod can be considered to be ‘fully saturated’, i.e., having a global recycling coefficient for hydrogenic species near unity.

The divertor structure is a baffled, ‘vertical plate’ design which is optimized to spread the power e-folding distance (1-4 mm, mapped to outer midplane) over the vertical portions of the divertor plates. A novel outer divertor bypass valve system [4,5] allows the neutral leakage from the divertor volume to the main chamber to be controlled dynamically during a discharge. Primary limiter structures in the main chamber consist of a toroidally continuous inner-wall limiter, and principally two discrete outboard limiters.

Neutral pressures are measured near the outer midplane, the vessel top, and in the divertor with Baratron and shielded Bayard-Alpert gauges. We monitor the total ionization in the main chamber by scaling from a single horizontal chordal measurement of D_α light emission at the midplane. The ionization source profile at the outer midplane is determined from the local profiles of Ly_α emissivity, n_e and T_e [6].

High resolution profiles of electron temperature and density on both sides of the separatrix are obtained from a combination of an edge Thomson scattering system [7] and two scanning probe systems: a vertical-scanning probe that samples plasma at a position 'upstream' from the entrance to the outer divertor, and a horizontal-scanning probe that records plasma

conditions 10 cm above the midplane [8]. Cross-field profiles of both parallel and *ExB* flows can be inferred utilizing the scanning Mach probes. By integrating the poloidal projection of these flows along the trajectory of the vertical-scanning probe, the ion flux directed towards the outer divertor throat, $\Gamma_{throat,i}$, can be derived [8]. Langmuir probes at both the outer divertor plate provide plasma density, temperature, and ion flux profiles across the divertor surface. The total ion flux to the outer divertor plate, $\Gamma_{Plate,i}$, is determined by poloidal and toroidal integration of the ion flux profiles.

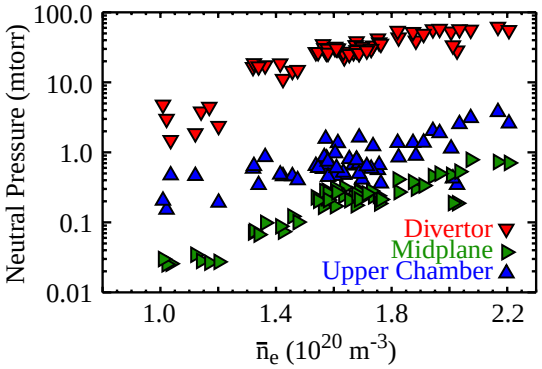

FIG. 1. Neutral pressures in divertor, upper chamber, and midplane locations vs. line-average electron density in Ohmic L-mode plasmas.

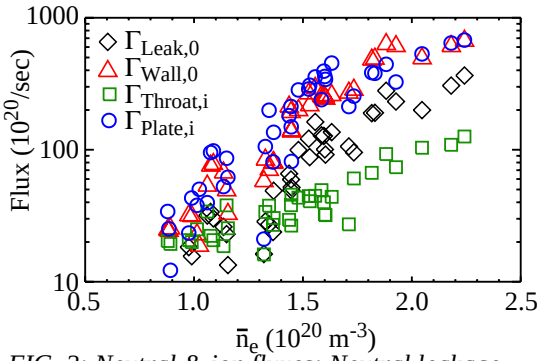

FIG. 2: Neutral & ion fluxes: Neutral leakage out of the divertor, $\Gamma_{Leak,0}$; Neutral flux towards the SOL, $\Gamma_{Wall,0}$; Ion flux entering the divertor, $\Gamma_{Throat,i}$; & Outer divertor ion flux, $\Gamma_{Plate,i}$.

3. The Midplane pressure

One central question of this study is the derivation, or origin, of the midplane pressure. Figure 1 shows the scaling of pressures at the midplane, divertor, and vessel top plotted vs $\bar{n}_e$. There are two likely sources of the neutral density at the midplane – (1) neutral leakage out of the high pressure divertor; and (2) neutrals created at the walls and surfaces outside the divertor due to cross-field ion fluxes. We designate any surface as a location where recycling occurs ‘outside' the divertor when neutrals, resulting from the recyling of ions on that surface, contribute to the SOL neutral density. This definition would include such surfaces as the semi-horizontal sections of the outer divertor plates in C-Mod, JET and ASDEX Upgrade (AUG). The vertical sections of those divertor plates, where the separatrix intersects the surface, would be considered 'inside' the divertor; neutrals created there must travel through 'leaks' in the structure to reach the outer SOL and midplane.

We cannot directly measure the divertor neutral leakage, $\Gamma_{Leak,0}$, but an estimate can be made based on divertor pressure and the conductance of known openings and assuming free molecular flow (see Figure 2). Other important ion and neutral flows shown in Figure 2 are: $\Gamma_{Plate,i}$, $\Gamma_{Throat,i}$, and $\Gamma_{Wall,0}$, the neutral flux entering the SOL from the wall based on pressure measurements in a horizontal port (assuming free-streaming neutrals to obtain a flux). All of

these estimates assume toroidal symmetry. Even though the upper vessel has 2-3 x the midplane pressure (Fig. 1) we assume poloidal symmetry and utilize the midplane pressure to estimate conservatively $\Gamma_{Wall,0}$.

All ion and neutral flows are of similar magnitude other than $\Gamma_{Throat,i}$, which is smaller. Because $\Gamma_{Leak,0} \sim \Gamma_{Wall,0}$, it is conceivable that neutral leakage from the divertor could explain the midplane pressure. However, there is some inconsistency among the measurements. We expect the flow into the divertor, $\Gamma_{Throat,i}$, to be significantly lower than the ion current to the plates based on divertor recycling, and it is. On the other hand we expect $\Gamma_{Throat,i} \geq \Gamma_{Leak,0}$, because, in steady state, the neutral loss out of the divertor through leakage or direct ionization across the X-point in the core, should be balanced by the ion flow back into the divertor. At the present time we are not able to reconcile these measurements with our understanding of divertor physics.

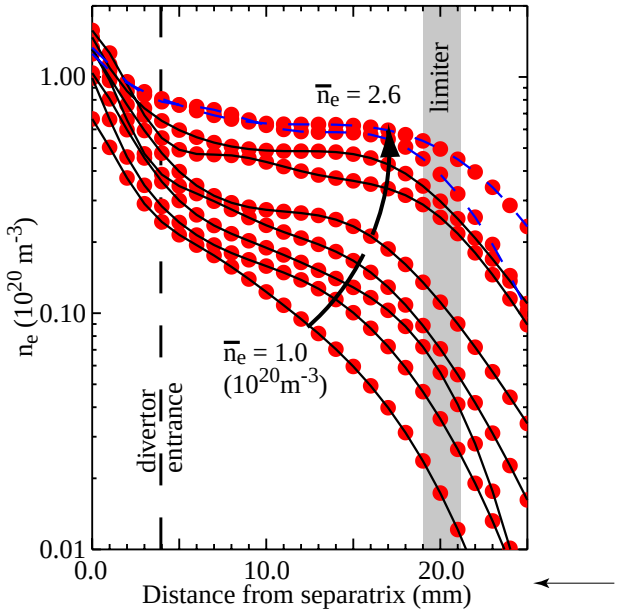

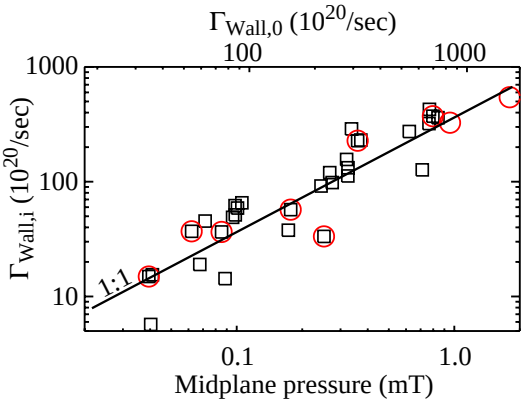

FIG. 4: Ion flux to the wall based on horizontal scanning probe measurements. All data have outer gaps ~ 18-22 mm. ◯- Same data as Fig. 3.

FIG. 3: density profiles in the SOL for a range in core conditions: $1 \leq \bar{n}_e \leq 2.6x10^{20}$, I_p ~ 800kA.

But let us examine the other source of midplane neutrals – ion flow to the walls. Figure 3 includes density profiles across the SOL for 9 different core densities ranging from 1.0 x10^{20} to 2.6x10^{20} m^{-3} ($0.17 \leq n/n_{Greenwald} \leq 0.45$), derived from the horizontal scanning probe. The limiter location, ρ_{Lim}, varied between 19 and 22 mm for these data. Flux surfaces in the range ~5 mm $\leq \rho \leq \rho_{Lim}$ impact on the horizontal section of the outer divertor plate (baffle section) and beyond, recycling outside the divertor. The density, and thus recycling, at the limiter, the limiter shadow, and outer divertor baffle surfaces are strongly dependent on the core density. At the two highest densities shown, the n_e profile near the separatrix has flattened such that n_{sep} has decreased with increasing $\bar{n}_e$. At even higher densities the data are less consistent, but in general the flat region of the profile continues to become broader, resulting in increased densities at the limiter.

Assuming that ionization can be neglected in the limiter shadow, then $\Gamma_{Wall,i}$ the perpendicular flux of ions across the flux surface delineated by the limiter edge, can be estimated from the data of Figure 3. The trajectory of the horizontal scanning probe passes between two limiter structures which are separated by 0.8 meters along magnetic field lines. Ionization can thus be neglected in the limiter-shadow particle balance. By integrating the ion saturation current profile across the shadow, the cross-field flux density entering the limiter-shadow ($\Gamma_{\perp}$) can be obtained. The particle flux onto the limiter/walls, $\Gamma_{Wall,i} = \Gamma_{\perp} \cdot A_{Sep}$, is shown in Fig. 4, plotted against the midplane pressure. We see that the ion flux to the limiter radius scales linearly with the midplane pressure (which itself scales as $\sim \bar{n}_e^4$; see Fig. 1). The top horizontal axis provides $\Gamma_{Wall,0}$ converted from the midplane pressure. Based on other measurements, $\Gamma_{Wall,i}$ underestimates the total wall recycling: analysis of D_α and Ly_α measurements indicates that recycling at the inner wall is 2-3 x that at the outer edge; upper vessel pressures are 2-3 times that at the midplane indicating higher levels of ion recycling there as well; flux surfaces in the region $5 \le \rho \le \rho_{Lim}$ impact on the horizontal section of the outer divertor leading to additional recycling.

Both $\Gamma_{Wall,i}$ and $\Gamma_{Leak,0}$ are likely contributing to the midplane pressure. Given the uncertainties in these measurements (particularly the inconsistencies between $\Gamma_{Leak,0}$, $\Gamma_{Throat,i}$ and $\Gamma_{Plate,i}$) we cannot at this time determine their relative contributions with confidence. However, due to the strong correlation of the direct measurement $\Gamma_{Wall,i}$ with P_{mid} we feel that ion fluxes dominate the generation of the midplane neutral population.

4. Wall and divertor fluxes

The 'strength' of main chamber recycling is a subjective assessment carried out in comparison with other fluxes. To assist in this discussion we define the following parameters: $\alpha = \Gamma_{Throat,i}/\Gamma_{Wall,i}$, and $\beta = \Gamma_{Plate,i}/\Gamma_{Wall,i}$. If wall recycling fluxes are of similar order to that

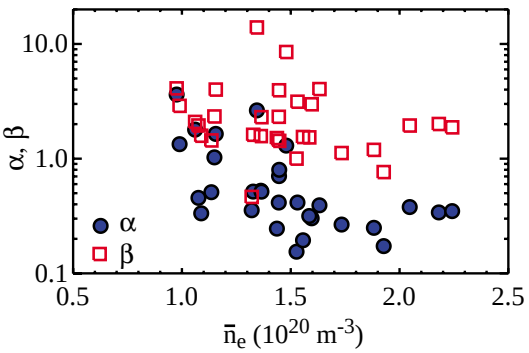

FIG. 5: Ratios of fluxes: $\alpha = \Gamma_{Throat,i}/\Gamma_{Wall,i}$; $\beta = \Gamma_{Plate,i}/\Gamma_{Wall,i}$. Outer gap range 18-22 mm.

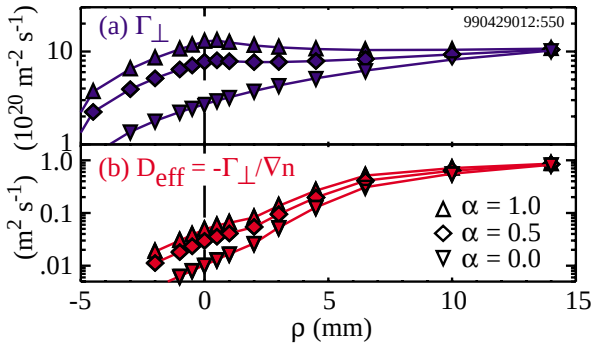

FIG. 6. Profiles of (a) cross-field particle flux density; and (b) effective particle diffusivity. The dependence on $\alpha = \Gamma_{Throat,i}/\Gamma_{Wall,i}$ is shown.

entering the divertor ($\alpha \sim 1$) then we know that the traditional picture of the divertor/SOL (all particle and heat flows travel to the divertor plate) is inaccurate. Even if $\alpha >> 1$ there are other reasons for efforts to understand the magnitude and cause of such wall fluxes: impurities generated at the outer midplane have a much higher probability (x10-100) of entering the core than those originating from the divertor [9]. The data of Fig. 5 indicate that α decreases with increasing $\bar{n}_e$, reaching values of $\alpha<1$ for most of the C-Mod operating regime. We also find that the ratio, $\beta = \Gamma_{Plate,i}/\Gamma_{Wall,i}$, is on the order of $\beta \sim 2–5$. Based on the discussion of Fig. 4 regarding $\Gamma_{Wall,i}$ and $\Gamma_{Throat,i}$, both α and β are overestimates. The value for α is consistent with past modelling [1] where the values for α were in the range .5 - .2 from low to high density operation. That model did not take into account leakage fluxes.

In summary, the ion flow to the main chamber walls is typically greater than the flow into the divertor for C-Mod divertor operation. The total flux to the wall approaches the total ion flux to the divertor plate at high density.

5. Cross-field particle transport

Utilizing the particle balance equation ($\nabla \cdot \Gamma = S_i$), the source ($S_i$) and n_e profiles, we derive the radial profiles of the perpendicular ion flux in the SOL ($\Gamma_\perp$) and the effective cross-field diffusivity, D_{eff} [8]. The local midplane ionization source (S_i) is derived from the measured local Ly_α emissivity [6,8], n_e and T_e profiles. The parallel ion flux to the divertor is varied parametrically as a fixed fraction, α, of the wall flux. Three values for α are assumed – 0.0, 0.5 and 1.0. Figure 6a shows typical resultant profiles for the cross-field flux, $\Gamma_\perp$, from an ohmic L-mode discharge (I_p = 0.8 MA, BT = 5.3 Tesla, $\bar{n}_e = 1.8 \times 10^{20}$ m^{-3}). Note that the value of $\Gamma_\perp$ at the separatrix correspondingly increases as α is increased. However, the value of $\Gamma_\perp$ at the wall is unaffected by the choice of α, since it is fixed by the measurements. The resultant effective particle diffusion coefficient, $D_{eff} = -\Gamma_\perp / \nabla n$, is also shown in Fig. 6b. This definition of D_{eff} is not meant to imply that the transport fluxes are 'diffusive'.

D_{eff} at the separatrix varies by a factor of 2 in going from α= 0.5 to 1. However, regardless of this variation in α, D_{eff} is seen to increase by an order of magnitude in the ~10 mm distance from the separatrix and be fairly independent of α, $\bar{n}_e$, and confinement regime. This radial variation is similar to that inferred by UEDGE modelling [1], yet the analysis technique and inputted data sets are quite different. The lowest values of D_{eff} near the separatrix are found in H-mode discharges. The values of D_{eff} in the far SOL appear to be roughly similar in both L- and H-mode regimes, and are high (factor of 10) compared to that predicted by Bohm diffusion.

It is also found that D_{eff} at a location close to the separatrix increases markedly with increasing collisionality (or increasing density), varying by an order of magnitude over the

density range of these discharges [8]. We have performed a regression analysis of D_{eff} at the ρ=2 mm location on local values of T_e (eV) and n_e(m^{-3}). The result is the following scaling:

$$D_{eff} \sim 0.069\ (T_e/50)^{-3.5}\ (n/10^{20})^{1.7}\ \ (m^2\ s^{-1}). \qquad (1)$$

This scaling agrees well with the D_{eff} values obtained using UEDGE, both in terms of trend and magnitude. Such a scaling as given in (1) is suggestive of a scaling with collisionality of the SOL plasma, $D_{eff} \sim \lambda_{ei}^{-1.7}$, where λ_{ei} is the electron-ion mean-free path. This scaling is found to apply to a region of the SOL reaching 5 mm from the separatrix.

6. Cross-field heat convection

The large values of D_{eff} in the far SOL, and at high $\bar{n}_e$, suggest that convection plays a significant role in heat transport, depending on density and collisionality. It is interesting to compare the resultant convected power crossing a given flux surface (Q_{conv}) to the power that must cross that flux surface (Q_{div}) in order to account for the parallel electron conduction losses to the divertor/baffle surface. Assuming $T_i \approx T_e$, the convected power is $Q_{conv} \sim 5A_{LCFS}\ T_e\Gamma_i$. An estimate of the power necessary to support electron parallel conduction losses in the SOL beyond the flux surface at location ρ is

$$Q_{div}(\rho) \approx A_{LCFS}\frac{4}{7}\frac{\kappa_0}{\pi^2 q^2}\int_{\rho}^{\rho_{limiter}} T_e^{7/2}(\rho')\partial\rho' \qquad (2)$$

where A_{LCFS} is the area of the last closed flux surface, and q is the safety factor. In Fig. 7a we plot Q_{conv} and Q_{div} for a low-density case ($\bar{n}_e$~1.2x10^{20}m^{-3}), where convection dominates only in the far SOL. For the high density case (b, $\bar{n}_e$~2.6x10^{20}m^{-3}, n/$n_{Greenwald}$ ~ 0.43), Q_{conv} has risen near the separatrix to values slightly higher than Q_{div}. The corresponding values of Q_{div} (0)/P_{SOL} (P_{SOL} is the total power crossing the separatrix) are ~ 15% and 40% for cases (a) and (b) respectively.

As collisionality is increased further beyond this range of data we expect further changes: (1) convective heat losses could potentially lead to a thermal transport limit at higher densities, perhaps playing a significant role in the density limit; and (2) the separatrix temperature will drop strongly as the balance of parallel conduction to the divertor with P_{SOL} ($T_{e,sep} \propto P_{SOL}^{2/7}$) no longer holds and convection dominates more completely.

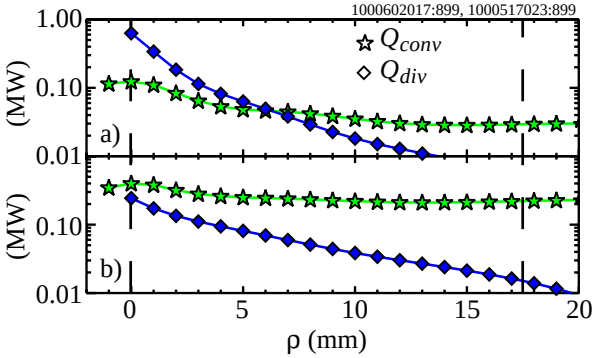

Fig. 7. Profiles of Q_{conv}, Q_{div} for $\bar{n}_e$= (a) 1x10^{20} m^{-3} and (b) 2.6x10^{20} m^{-3}. Dashed lines indicate the separatrix (ρ=0) and limiter locations.

7. Effect of the Divertor Bypass on Fuel and Recycling Impurities

In an effort to understand better main chamber recycling and impurity transport we have utilized the divertor bypass which can open or close between, or even during discharges in times as short as ~ 20 ms. This *in situ* control of the mechanical conductance between the divertor and the main chamber allows precise and unambiguous experiments, avoiding traditional problems in this type of investigation associated with comparing discharges from different run periods.

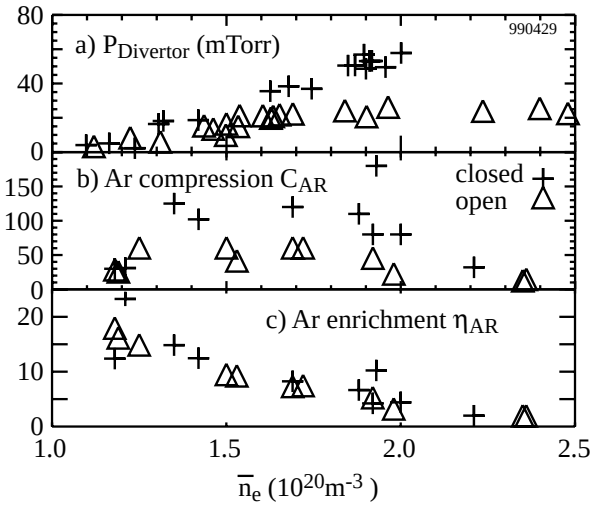

Fig. 8: Effect of opening the divertor bypass on a) Divertor pressure; b) argon compression; and c) argon enrichment.

With respect to the hydrogenic neutral particle behavior, the divertor pressure is reduced by a factor of ~ 2 when the bypass is open (Fig. 8a), with no change in the main chamber pressure. These results, obtained in Ohmic discharges, are generally obtained in all C-Mod discharges, including H-modes. The weak dependence of the main chamber pressure on the divertor leakage conductance is surprising, but is consistent with a fixed leakage flux (e.g. when the bypass is opened the conductance is doubled, but the driving pressure is approximately halved) [5]. The dependence is further weakened by the large amount of main chamber recycling discussed above.

The divertor bypass can also strongly affect the compression of recycling impurities into the divertor. According to convention, we define impurity compression C_Z as $n_{Z,0}$(div)/ $n_{Z,i}$(core), where $n_{Z,0}$(div) is the neutral impurity density in the divertor derived with a residual gas analyzer (RGA) and $n_{Z,i}$(core) is the impurity ion density in the core plasma derived by spectroscopic means. Similar to the deuteruim behavior, the divertor bypass reduces the compression of argon (Fig. 8b) by a factor of ~ 2, resulting in no change to the enrichment = C_Z/C_D (Fig. 8c), although the latter decreases with discharge density. As with deuterium, an argon leakage flux which is independent of the leakage condutance is indicated.

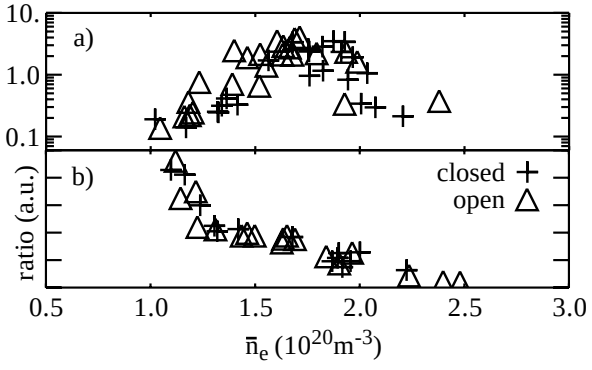

Fig. 9: Effect of opening the divertor bypass on the ratios: a) divertor brightness(ArII)/ core n_{Ar}; and b) $n_{Target}/\bar{n}_e$.

While the compression of deuterium and argon gas in the divertor is enhanced by reducing the leakage conductance (i.e. having the bypass closed), a critical issue from the point of view of radiative divertors is the resulting effect on the argon ion concentration in the divertor plasma. In this case, relative changes can be monitored using divertor Ar II line emission. Fig. 9a gives the ratio of divertor Ar II emission to the central argon ion density. One can see that the bypass has no effect on this ratio, although the discharge density changes the Ar II brightness. Fig. 9b shows that similarly, the bypass has no effect on the divertor target plasma density for a given discharge density (similarly for the divertor D_α, not shown).

The results of Fig. 8 and Fig. 9 are consistent with a scenario where the neutral leakage flux is limited by the flux of ions onto the divertor plates, and the escape probability of the resulting atom into the private flux region—a so called "flux-limited" scenario. The ion flux in turn is controlled by the SOL plasma conditions and the resulting divertor gas pressures are determined by the leakage conductance. Therefore a disconnect exists between the divertor gas pressure and the divertor ion density/flux. While this picture is supported by simple modeling in the case of deuterium [5], the expectations for argon are not clear and require more study.

Based on modelling of the divertor plasma and neutrals [5], we believe that the 'flux-limited' feature of the C-Mod divertor is a consequence of a relatively high leakage conductance,

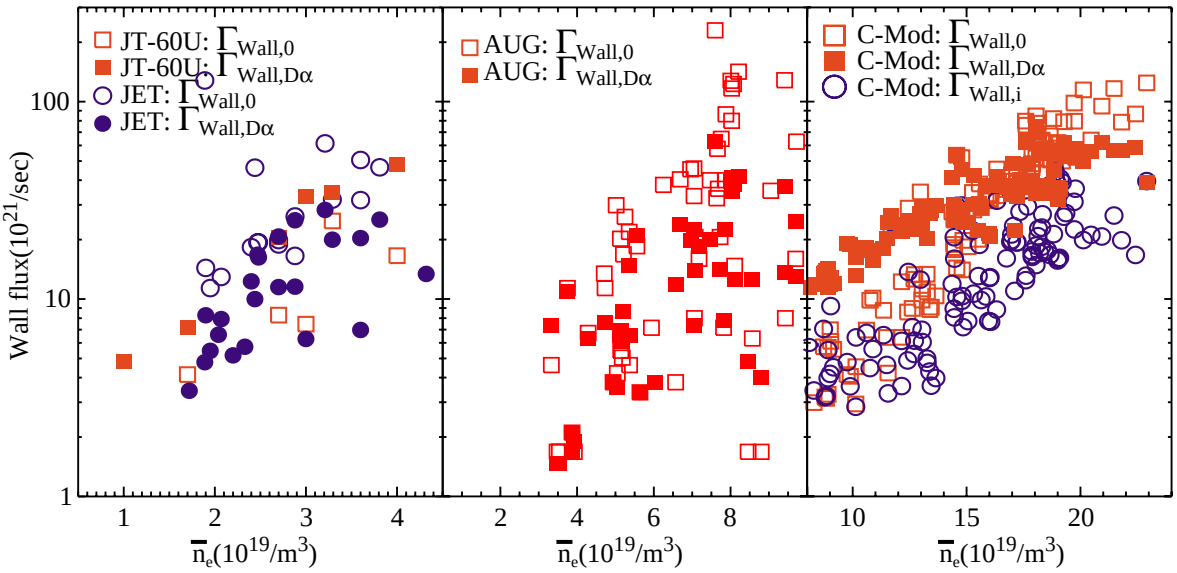

Fig. 10: Scaling of the integrated wall flux for (a) JT-60U and JET; (b) ASDEX UG; and c) C-Mod. The different measures of integrated wall flux shown are derived from the midplane pressure ($\Gamma_{Wall,0}$), midplane D_α ($\Gamma_{Wall,D\alpha}$), and ion flux to the limiter radius ($\Gamma_{Wall,i}$).

e.g. compared to the divertor throat conductance. These results imply that improvements in both fuel and impurity compression/screening may still be had by significant reductions in the leakage conductance. At small enough leakage conductance a different regime is expected,

'conductance-limited' leakage, where the leakage fluxes are proportional to the conductance and the divertor gas pressures are independent [5].

8. Comparison of Alcator C-Mod with other devices

The data presented in the previous sections naturally bring to mind the following question: Are these results unique to C-Mod? We have made an effort to collect data from several experiments in a very limited manner for comparison with C-Mod. Figure 10 shows the scaling of the integrated radial fluxes obtained from 4 experiments – a) JT-60U (Open divertor) [10, 11] and JET (MKI, MKII, MKIIGB) [12]; b) ASDEX UG (LYRA divertor) [13]; and c) C-Mod. In addition to the variables described earlier, $\Gamma_{Wall,0}$ and $\Gamma_{Wall,i}$, we also plot $\Gamma_{Wall,D\alpha}=B_{D\alpha}\cdot 20\cdot A_{sep}$. $B_{D\alpha}$ is the midplane D_α brightness, A_{sep} is the plasma surface area and 20 the number of ionization/D_α photon. In all cases the integrated midplane fluxes scale strongly with $\bar{n}_e$ in a similar manner. The results of the different measurement methods agree to factors of 2-5.

A surprising result is that the magnitudes of the fluxes are similar for machines of very different size! Ignoring differences of measurement techniques we plot the particle flux density, $\Gamma_{mid}=\Gamma_{wall}/A_{sep}$ in Figure 11. A scaling of $\Gamma_{mid} \sim \bar{n}_e^2$ would be consistent with all tokamaks. There is not anything obvious from either Fig. 10 or 11 indicating C-Mod is substantially different from other tokamaks. However, further work is needed to make more direct measurements of ion fluxes to the wall and divertor of these experiments in order to make a better comparison.

8. Summary

In exploring the potential sources of the midplane pressure we find that both the flux of neutrals escaping the divertor through 'leaks' in the divertor structure, and ion recycling on main chamber surfaces, appear to contribute. We are not able to determine what the relative contribution of each of these sources is to the midplane pressure but it appears that ion recycling in the main chamber is dominant, particularly at high densities. The recycling in the main chamber is evidenced by a flat

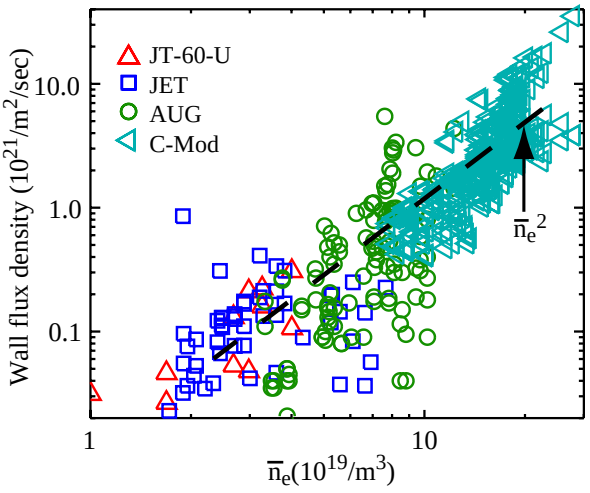

Fig. 11: Scaling of the particle flux density at the wall for 4 divertor tokamaks. The wall flux density is based on all the measurements of Fig. 10 taking into account the surface area of the separatrix.

'shoulder' in the SOL density profile, leading to fluxes on limiters and on the horizontal, or baffle, sections of the outer divertor. The density profile shoulder becomes flatter with increasing $\bar{n}_e$, enhancing this effect.

Using a conservative measure of the wall recycling we find that the ion fluxes to main chamber surfaces (outside the divertor) are larger than the flux entering the divertor and comparable to the divertor plate ion flux. This is a quantitative measure of the strength of the main chamber recycling, which, at least in the case of C-Mod, shows that the 'ideal' picture of divertor operation does not universally hold. The cause of these high ion fluxes to surfaces far out in the SOL is an enhancement in cross-field transport as the core plasma density is increased. The effective diffusion coefficient, derived from data, is low near the separatrix, rising to a value of D_{eff} ~10xD_{Bohm} in the far SOL. The different scaling of D_{eff} with $\bar{n}_e$ near, and far from the separatrix, may indicate that different transport mechanisms are dominant in those regions.

In analyzing the heat transport corresponding to the observed changes in D_{eff} we find that perpendicular heat convection is significant even at low densities, rising to a dominant role at $n_e/n_{Greenwald}$ ~ 0.45. The strength of this convective heat transport has implications for the separatrix T_e and the density limit.

Acknowledgements

This C-Mod work was supported by the U.S. Dept. Of Energy under grant DE-FC02-99ER54512. The JET work was carried out under the European Fusion Development Agreement as part of the JET work-programme.

References

[1] UMANSKY, M.V., et al., Phys. Plasmas **6** (1999) 2791.
[2] BOSCH, H.S., et al., J. Nucl. Mater. **220-220** (1995) 558.
[3] HUTCHINSON, I.H., et al., Phys. Plasmas **1** (1994) 1511.
[4] PITCHER, C.S., et al., Phys. Plasmas **7** (2000) 1894.
[5] PITCHER, C.S., et al., accepted to J. Nucl. Mater.
[6] BOIVIN, R.L., et al., Phys. Plasmas **7** (2000) 1919.
[7] MOSSESSIAN, D. et al., 'High resolution edge Thomson scattering measurements on the Alocator C-Mod tokamak', accepted to Rev. Sci. Instrum.
[8] LaBOMBARD, B. et al., 'Cross-field plasma transport and main chamber recycling in diverted plasmas on Alcator C-Mod', accepted to Nucl. Fusion.
[9] LIPSCHULTZ, B. et al., 'A study of molybdenum influxes and transport in Alcator C-Mod', submitted to Nucl. Fusion.
[10] ASAKURA, N., et al., J. Nucl. Mater., **241-243**, (1997) 559-563 .
[12] HORTON, L.D., VLASES, G.C., ANDREW, P., et al., Nucl. Fusion **39** (1999) 1.
[13] KALLENBACH, A., et al., Plasma Phys. Control. Fusion **41** (1999) B177.